Title

Efficient solar-to-fuels production from a hybrid microbial–water-splitting catalyst system

Journal

Proceedings of the National Academy of Sciences of the United States of America, 112(8)

ISSN

0027-8424

Authors

Torella, Joseph P
Gagliardi, Christopher J
Chen, Janice S
et al.

Publication Date

2015-02-24

DOI

10.1073/pnas.1424872112

Peer reviewed

Efficient solar-to-fuels production from a hybrid microbial–water-splitting catalyst system

Joseph P. Torella[a,1], Christopher J. Gagliardi[b,1], Janice S. Chen[a], D. Kwabena Bediako[b], Brendan Colón[a], Jeffery C. Way[c], Pamela A. Silver[a], and Daniel G. Nocera[b,2]

[a]Department of Systems Biology, Harvard Medical School, Boston, MA 02115; [b]Department of Chemistry and Chemical Biology, Harvard University, Cambridge, MA 02138; and [c]Wyss Institute for Biologically Inspired Engineering, Harvard University, Boston, MA 02115

Contributed by Daniel G. Nocera, December 30, 2014 (sent for review December 8, 2014)

Photovoltaic cells have considerable potential to satisfy future renewable-energy needs, but efficient and scalable methods of storing the intermittent electricity they produce are required for the large-scale implementation of solar energy. Current solar-to-fuels storage cycles based on water splitting produce hydrogen and oxygen, which are attractive fuels in principle but confront practical limitations from the current energy infrastructure that is based on liquid fuels. In this work, we report the development of a scalable, integrated bioelectrochemical system in which the bacterium *Ralstonia eutropha* is used to efficiently convert CO_2, along with H_2 and O_2 produced from water splitting, into biomass and fusel alcohols. Water-splitting catalysis was performed using catalysts that are made of earth-abundant metals and enable low overpotential water splitting. In this integrated setup, equivalent solar-to-biomass yields of up to 3.2% of the thermodynamic maximum exceed that of most terrestrial plants. Moreover, engineering of *R. eutropha* enabled production of the fusel alcohol isopropanol at up to 216 mg/L, the highest bioelectrochemical fuel yield yet reported by >300%. This work demonstrates that catalysts of biotic and abiotic origin can be interfaced to achieve challenging chemical energy-to-fuels transformations.

bioelectrochemistry | isopropanol | biofuel | renewable energy | *Ralstonia*

Photovoltaics (PV) provide a scalable and cost-effective method for converting solar energy into electricity but do so only intermittently as a result of daily variations in solar intensity and the diurnal solar cycle (1–3). PV-based fuel generation can be used to bridge the gap between peak solar power and utility load curves (2, 4, 5), the simplest example of which is PV-driven water splitting to generate hydrogen as a fuel. A current lack of distribution and storage infrastructure for H_2, however, has led to slow technology adoption and thus H_2 is not yet widely used directly as a transportation fuel or for electricity generation via fuel cells (6, 7). Liquid fuels are more appealing as a solar storage medium because of their attractive energy density and existing sophisticated distribution and storage infrastructures (2). However, attempts to produce liquid fuel directly via CO_2 reduction have poor specificity and energy efficiency (8, 9) with exceptions only recently emerging (10–13).

An alternative approach to the direct reduction of CO_2 to liquid solar fuels is to engineer fuel production in organisms that naturally use light energy to fix CO_2 to biomass (14–16). Notwithstanding, photosynthetic organisms suffer inefficiencies arising from nonideal light-harvesting properties that are not likely to be addressed in the near term (17). As a result, the observed solar-to-biomass efficiency by plants typically approach only 1% of the thermodynamic maximum annually (18, 19) or between 1.4% and 2.0% over the growing season when calculated on the basis of total solar radiation (17).

In principle, the unique advantages of PVs and photosynthetic carbon fixation may be coupled to achieve higher solar-to-fuel efficiency (SFE), and several proof-of-principle demonstrations of this kind of coupling have been made. Electrolysis of biological culture media has been used to drive O_2 generation at the anode and, in most reports, H_2 or formate generation at the cathode (20–22). Hydrogen-oxidizing autotrophs grow on the evolved hydrogen or formate, producing biomass and, in one case, fusel alcohols (22). In other cases, the cathode may be used to deliver reducing equivalents directly to a target autotroph (23, 24) or indirectly via a soluble mediator such as Fe^{3+} or NO_2^-, which serves as the electron donor to the autotrophic microbe of interest (25, 26). In all cases, coupling these systems to a PV may enable solar-to-biomass and solar-to-fuel production (2, 27, 28).

These early demonstrations of electricity-driven carbon fixation have highlighted significant impediments to the design of scalable and high SFE systems. Some promising bioelectrosynthetic systems rely on obligate anaerobic bacteria that must be kept separate from the oxygen-generating anode, making them difficult to incorporate into such an integrated system (24). For systems incorporating aerobic bacteria, a prominent impediment is the ability to implement the oxygen evolution reaction (OER) efficiently in the pH-neutral environment commonly required for biological growth. To operate in water, precious metal catalysts such as platinum or indium have been used to drive the OER. Aside from the inherent limitations imposed by the criticality of such metals (29), these metals are inferior catalysts for water splitting under biologically amenable conditions. Although the minimal thermodynamic potential required for water splitting is 1.23 V (30), previous studies have operated at total cell potentials of 4.0–5.5 V (20–22) to drive biological growth, wasting 70–80% of input energy. This inefficiency is in part due to the high overpotentials required by these metal catalysts in driving the OER.

Significance

Renewable-fuels generation has emphasized water splitting to produce hydrogen and oxygen. For accelerated technology adoption, bridging hydrogen to liquid fuels is critical to the translation of solar-driven water splitting to current energy infrastructures. One approach to establishing this connection is to use the hydrogen from water splitting to reduce carbon dioxide to generate liquid fuels via a biocatalyst. We describe the integration of water-splitting catalysts comprised of earth-abundant components to wild-type and engineered *Ralstonia eutropha* to generate biomass and isopropyl alcohol, respectively. We establish the parameters for bacterial growth conditions at low overpotentials and consequently achieve overall efficiencies that are comparable to or exceed natural systems.

Author contributions: J.P.T., C.J.G., J.S.C., D.K.B., B.C., J.C.W., P.A.S., and D.G.N. designed research; J.P.T., C.J.G., J.S.C., D.K.B., and B.C. performed research; J.P.T., C.J.G., P.A.S., and D.G.N. analyzed data; and J.P.T., C.J.G., J.C.W., P.A.S., and D.G.N. wrote the paper.

The authors declare no conflict of interest.

Freely available online through the PNAS open access option.

[1]J.P.T. and C.J.G. contributed equally to this work.

[2]To whom correspondence should be addressed. Email: dnocera@fas.harvard.edu.

This article contains supporting information online at www.pnas.org/lookup/suppl/doi:10.1073/pnas.1424872112/-/DCSupplemental.

The ability to perform OER at low overpotential in neutral pH ranges (pH 6–8) has been achieved with the development of a cobalt phosphate (CoP_i) catalyst (31). This OER catalyst features many of the properties of the oxygen-evolving catalyst of photosystem II (PSII) including its structure (32–34) and its ability to self-assemble (35, 36), repair itself (37), and manage the proton-coupled electron transfer chemistry of water splitting akin to the Kok cycle of PSII (38). Of pertinence to this study, the catalyst can perform OER in natural waters of a wide variety of solution environments including buffers capable of supporting biological growth (39). When the CoP_i OER catalyst is coupled to a hydrogen evolution reaction (HER) catalyst (40), the evolved hydrogen is available for combination with CO_2, providing a foundation for the development of new biological, H_2-based CO_2 reduction strategies to produce liquid and solid fuels.

In this work, a fully integrated microbial–inorganic system has been engineered based on the CoP_i water-splitting anode, with NiMoZn or stainless-steel (SS) 304 mesh 60 cathodes to generate O_2 and H_2 (41), which has in turn been used to fix carbon to biomass in wild-type (wt) *Ralstonia eutropha* H16 and to isopropanol in an engineered strain of *R. eutropha*, *Re*2133-pEG12. For the former, a maximal bioelectrochemical efficiency of 17.8% is achieved for biomass, and for the latter a maximal bioelectrochemical efficiency of 3.9% is achieved for isopropanol. This bioelectrochemical isopropanol fuel yield (216 mg/L) is the highest yet reported. These high efficiencies are a result of the ability to perform water splitting at lower cell voltages owing to the more efficient OER and HER catalysis.On this point, the higher voltage needed for previous bioelectrochemical cells has been identified to originate from the inability to support water splitting vs. reactive oxygen species (ROS) generation at lower potentials. When water splitting is not prevalent, current is redirected to drive parasitic reactive side reactions that generate ROS, which leads to cell death. This work lays a foundation for realizing liquid fuel production based on solar water splitting and provides an important and general proof-of-principle demonstration that inorganic and biological materials can be interfaced to achieve solar-to-fuels storage schemes that are not realized by either system in isolation. Moreover, it shows that integrated inorganic–biological hybrid systems may offer yields beyond those available to photosynthetic organisms for the production of fuels.

Results

Bioelectrochemical Growth of *R. eutropha* H16 Driven by Earth-Abundant Water-Splitting Catalysts. A schematic of the system and the cell configuration used for the bioelectrochemical experiments is shown in Fig. 1. *R. eutropha* was cultured in the cell using a CoP_i anode and either NiMoZn electrodeposited on SS 304 mesh or plain SS mesh as a cathode. These electrodes furnished oxygen and hydrogen, respectively, which was the sole source of biological reducing equivalents. The electrolyte was a chloride-free minimal growth medium buffered at pH 7.0 with 36 mM phosphate (*Materials and Methods*), and the solution was saturated with gaseous CO_2. The cell voltage, E_{cell}, was operated in the range of 1.8–3.0 V, with current densities ranging between 0.5 and 11 mA/cm^2.

The potential E_{cell} required for water-splitting current in excess of 2 mA/cm^2 was between 2.0 and 2.3 V (*SI Appendix*, Fig. S1), which is higher than the potentials needed for the CoP_i | NiMoZn system in buffer solutions for two reasons. First, the solution resistivity of the growth medium was measured to be significantly higher (Ω_{soln} = 62.4 Ω) than normal water-splitting conditions owing to a relatively low overall salt concentration; the solution resistance translates to a solution voltage of ~0.5 V at 4 mA/cm^2 of current. Second, in the presence of the growth medium, the OER (η_{OER}) and HER (η_{HER}) overpotentials are higher than in buffered solutions. The η_{OER} was determined from the Tafel plot for CoP_i in the growth media (*SI Appendix*, Fig. S2) to be η_{OER} = 0.56 V vs. 0.53 V (at 4 mA/cm^2) in 0.1 M KP_i (pH 7.0) for typical water-splitting conditions. Using the foregoing measured values and thermodynamic values for OER and HER of $E^{\circ\prime}_{OER}$ = 0.815 and $E^{\circ\prime}_{OER}$ = –0.413 V vs. NHE, respectively, at pH 7, the η_{HER} may be determined from the following:

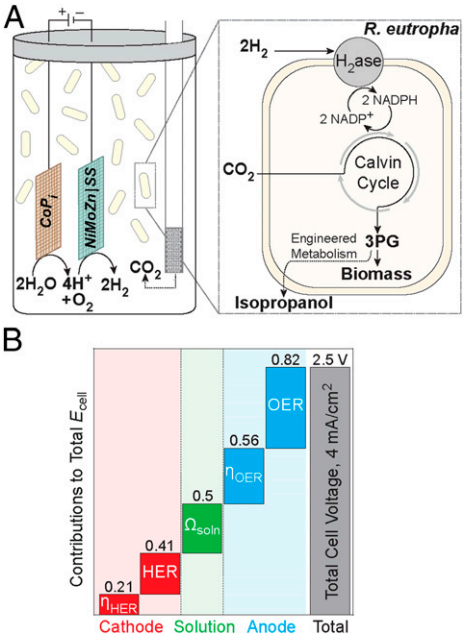

Fig. 1. Schematic diagram of bioelectrochemical cell. (*A*) Water oxidation takes place at the cobalt phosphate (CoP_i) anode with proton reduction taking place at the nickel molybdenum zinc (NiMoZn) or stainless-steel (SS) cathode. CO_2 is continuously sparged into the cell. The wild-type (wt) bacterium *Ralstonia eutropha* (*Re*) H16 oxidizes H_2 using oxygen-tolerant hydrogenases (H_2ase) to generate reduced cofactors (e.g., NADPH) and ATP, and uses these to reduce CO_2 to 3-phosphoglycerate (3PG) via the Calvin cycle. 3PG is then converted into biomass in wt *Re*H16 or may be diverted in metabolically engineered *Re*2133-pEG12 into isopropanol. (*B*) Voltage contributions from CoP_i and NiMoZn water-splitting half-reactions, including overpotentials (η), and solution resistance (Ω_{soln}) components for a system driven at E_{cell} = 2.5 V to achieve a current density of ~4 mA/cm^2 (averaged over 5 d).

$$\eta_{HER} = E_{cell} - \left[\left(E^{\circ\prime}_{OER} + \eta_{OER}\right) + \Omega_{soln} + E^{\circ\prime}_{HER}\right]. \quad [1]$$

The relative contributions of the CoP_i anode, NiMoZn cathode, and solution resistivity to the overall cell potential, E_{cell} = 2.5 V, operating at a current density of 4 mA/cm^2 is schematically summarized in Fig. 1*B*.

We observed consistent growth of *R. eutropha* for $E_{cell} \geq 2.7$ V (Fig. 2 *A* and *B*). Growth at 2.3 V is achievable after an extended lag phase, and occasionally a long lag phase is observed even at higher voltages (data not included in Fig. 2*A*). We note that CoP_i | NiMoZn electrodes and *R. eutropha* were reciprocally compatible under applied potentials: CoP_i and NiMoZn electrodes permitted biological growth, and conversely, biological growth did not oppose long-term catalyst function. Neither the range of salts contained in *R. eutropha* minimal medium nor the presence of biological material greatly altered electrode performance, as cell current was relatively stable (*SI Appendix*, Fig. S3) and declined by <50% over 14 d.

Cathode-Derived ROS in Bioelectrochemical Reactors. We sought to understand the loss of cell viability at E_{cell} < 2.7 V by examining

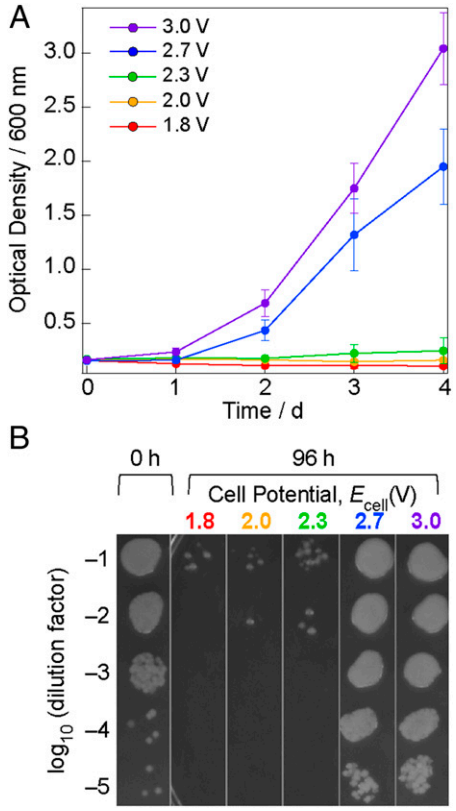

Fig. 2. Cell growth of *R. eutropha*. (*A*) Time course of *R. eutropha* cell growth by monitoring OD at 600 nm, using a CoP_i anode and NiMoZn cathode poised at a range of total cell potentials (E_{cell}); currents obtained at each of these cell potentials are shown in *SI Appendix*, Fig. S1. Error bars represent SEM with n = 3–5 independent experiments at each potential. (*B*) Spot assays of *R. eutropha* before starting electrolysis (0 h), and after 96 h of electrolysis with CoP_i/NiMoZn electrodes, as a function of E_{cell}.

cell cultures in a three-compartment H cell. As established by the spot assays from its cathodic and anodic chambers (Fig. 3*A*), toxicity occurred exclusively at the cathode for cell potentials poised at a significant water-splitting underpotential (1.8–2.1 V). Moreover, for electrolysis carried out in the single-cell configuration of Fig. 1*A*, toxicity is significantly reduced by sparging the cell culture with CO_2 to eliminate excess oxygen (Fig. 3*B*). We also confirmed the production of ROS at water-splitting underpotentials. Specifically, as shown in Fig. 4*A*, H_2O_2 is detected in the cathode compartment of an H cell but not in the anode compartment. In a single-cell configuration, H_2O_2 production rate increases monotonically with decreasing potential and is an order of magnitude greater at 2.1 V than at 2.6 V (*SI Appendix*, Fig. S4).

The electrolysis experiment was repeated while supplementing the cathodic compartment with 400 μg/mL of an H_2O_2-decomposing enzyme, bovine liver catalase. As shown in Fig. 4*A*, the addition of catalase decreased H_2O_2 to undetectable levels. An identical experiment using heat-inactivated bovine liver catalase had little effect on the H_2O_2 concentration. Parallel to these concentration measurements, cell viability was measured. As shown in Fig. 4*B*, catalase addition was sufficient to rescue cell viability at this low E_{cell}; however, this effect was attenuated for the addition of heat-inactivated catalase. These experiments together establish that enzymatically competent catalase was capable of restoring full cell viability, and furthermore establish a direct link between H_2O_2 availability and cell death, suggesting that cathodically generated H_2O_2 is a major cause of toxicity at low E_{cell}.

While performing these experiments, we observed low levels of toxicity originating from the NiMoZn cathode in the absence of an applied potential (*SI Appendix*, Fig. S5). We believe this is due to the ability of this electrode to generate ROS species at open circuit, likely due to the chemical oxidation of the metals by oxygen to produce H_2O_2. Consistent with this contention, *R. eutropha* cultures subject to the NiMoZn cathode at open circuit potentials and incubated with catalase were noticeably healthier compared with samples without catalase (*SI Appendix*, Fig. S5). Accordingly, we replaced the cathode with the inert albeit slightly less active HER electrode, a plain SS 304 mesh cathode (6.0 ± 0.2 mA/cm^2 for NiMoZn vs. 2.6 ± 0.2 mA/cm^2 for SS at 2.7 V). The cell growth for SS is similar to that of NiMoZn (*SI Appendix*, Fig. S6), but it exhibits slightly better behavior (steeper cell growth, shorter average lag phase duration, and less variable growth kinetics) as a result of reduced ROS generation. Similar biomass production could also be obtained with the SS cathode despite its lower HER performance. The SS cathode was therefore used for subsequent experiments.

Bioelectrochemical Production of Fusel Alcohols by Genetically Engineered *R. eutropha*. Wild-type *R. eutropha* H16 was replaced with *Re*2133-pEG12 in the bioelectrochemical cell shown in Fig. 1. The strain, engineered by Grousseau et al. (42), produces isopropanol at high yield under fructose-fed, nutrient-limited conditions. As summarized in Fig. 5*A*, whereas wt *R. eutropha* rapidly converts acetyl-coenzyme A (acetyl-CoA) to the storage polymer polyhydroxybutyrate (PHB) under nutrient-limited growth conditions (43), *Re*2133-pEG12 is disrupted in PHB synthesis and expresses four genes that redirect acetyl-CoA toward the synthesis of isopropanol. Plasmid pEG12 constitutively expresses genes for a ketothiolase (*phaA*) and acetoacetyl-CoA transferase (*ctf*) from *R. eutropha*, and an acetoacetate decarboxylase (*adc*) and alcohol dehydrogenase (*adh*) from *Clostridium* sp. (in red). Both the native *phaA* and a plasmid-encoded copy of phaA (*phaA**) are expressed in this strain, which has also been shown to produce the side products pyruvate and acetone.

*Re*2133-pEG12 grew robustly in our electrochemical setup and, over the course of 5 d, produced 216 ± 17 mg/L isopropanol (Fig. 5*B*), which is the highest yield of fuel reported for a bioelectrochemical system (22). Isopropanol production was highly selective (~90% yield), as only small quantities of acetone (10 ± 1 mg/L) and pyruvate (17 ± 7 mg/L) were detected in the medium after 120 h. Minimal medium was amended with 0.05% ammonium sulfate to limit cell growth to ~0.8 g/L (42) [optical density (OD) ~ 2.0], consistent with the final OD of ~2.5 for the cultures. Cessation of growth due to nitrogen depletion was followed by a rapid increase in isopropanol production. This

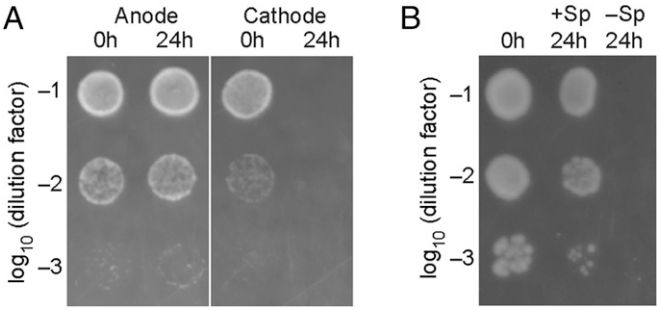

Fig. 3. Spot assays to determine cell toxicity. Spot assays of *R. eutropha* viability following 24 h of electrolysis performed galvanostatically at 0.5 mA/cm^2 (1.8–2.1 V) using CoP_i and NiMoZn electrodes: (*A*) from the cathodic and anodic chambers of an H-cell and (*B*) from a single cell chamber with (+Sp) and without (–Sp) continuous sparging of CO_2.

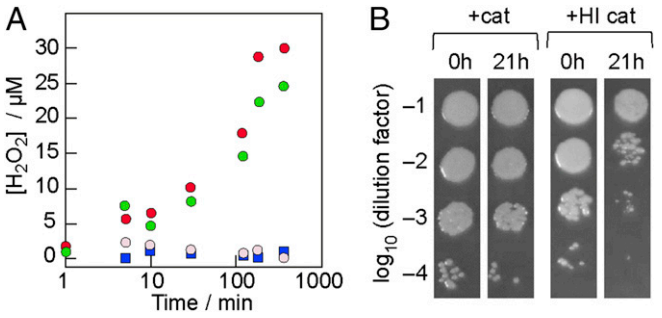

Fig. 4. Effect of catalase on cell viability. (*A*) Measurement of H_2O_2 production: in anode (blue squares) and cathode (red circles) of an H cell subjected to electrolysis performed galvanostatically at 1 mA (E_{cell} = 1.8–2.1 V); and in the cathode with the addition of bovine liver catalase (cat) (gray circles) or heat-inactivated bovine liver catalase (green circles). (*B*) Accompanying spot assays of *R. eutropha* viability in the cathodic chamber of an H cell run galvanostatically at 1 mA, 1.8- to 2.1-V cell potential with the addition of 400 μg/mL active (+cat) or heat-inactivated (+HI cat) bovine liver catalase.

decoupling of growth and product synthesis is consistent with the previously reported behavior of this strain under fructose-fed conditions (42) and with pyruvate synthesis kinetics in other PHB^- strains of *R. eutropha* (44).

Discussion

The CoP_i OER catalyst permits water splitting to be performed in biologically compatible solutions and at operating potentials significantly lower than those used in previous bioelectrochemical studies. Specifically, we have shown that the potential used to support biological growth can be decreased by >1.3 V and that platinum and other rare earth metal electrodes are dispensable.

The ability to achieve bacterial growth at lower potential has revealed a quizzical dependence of biological viability on cell potential at both high ($E_{cell} \geq 4.0$ V) and low ($E_{cell} \leq 2.3$ V) potentials. The loss of cell viability at high potentials has been ascribed logically to the production of ROS via water oxidation at the anode, where oxygen is normally produced in the water-splitting reaction (20, 22). Additionally, it is worth noting that anodic oxidation of chloride at cell potentials of 1.36 V generates highly toxic hypochlorite. Although this has long been recognized (20, 21), it likely contributes to toxicity in recent studies where chloride has been included in the medium. To minimize these deleterious anodic reactions on cultures, various methods have been pursued including multichamber cell designs, and anodic shielding to limit toxicity of electrogenerated species (22). However, we show here that a distinct mechanism operates at low potentials, where ROS, and specifically H_2O_2, are produced via oxygen reduction at the cathode, rather than by water oxidation at the anode. The latter mechanism imposes a limit on cell potential and is therefore the more serious challenge in building high-efficiency bioelectrochemical systems.

The origin of ROS toxicity at the cathode may be understood by considering the redox potentials shown in Fig. 6. At pH 7, the production of superoxide ($O_2^{\cdot -}$), hydrogen peroxide (H_2O_2), and hydroxyl radical ($HO^{\cdot}$) are all thermodynamically favored compared with the HER couple and thus will be generated at any potential high enough to drive proton reduction (45). Although we identified a role for H_2O_2 in cellular toxicity, superoxide and hydroxyl radicals may play a role as well. Due to their favorable thermodynamics, ROS production rates will be favored over H_2 production at underpotentials to the water-splitting reaction. More generally, lower potentials will increase the faradaic efficiency of ROS production at the expense of H_2 production (*SI Appendix*, Fig. S4). The onset potential of cell growth will be the potential at which H_2 production, which supports cell growth, is sufficient to outweigh the toxic effects of ROS production. In our case, the observed onset potential for cell growth is 2.3 V > $E_{cell} \geq$ 2.7 V.

Within the context of Eq. **1**, the use of noble metal electrodes in pH 7 cell medium results in a high η_{OER}, and hence higher potentials may be required to achieve water splitting and circumvent ROS production. In the cell shown in Fig. 1, the substantial decrease in η_{OER} by CoP_i allows for a significantly lower E_{cell} potential to be achieved. Indeed, in the cell configuration shown in Fig. 1, the η_{HER} and Ω_{soln} are larger contributors to E_{cell} than η_{OER}.

The lower E_{cell} for the CoPi | NiMoZn or SS water-splitting system is manifested in higher overall solar-to-fuels efficiencies. For an integrated bioelectrochemical setup that uses solar energy to drive water splitting, followed by biological utilization of the evolved H_2 to produce biomass or isopropanol fuel, the output biomass (B) in milligrams dry cell weight (mgDCW) or isopropanol (I_P) in milligrams is given by the following:

$$B = W \times (52\ \text{mgDCW/kJ}) \times \eta_{V_{th}} \times \eta_{H_2} \times \eta_{bio}, \quad [2]$$

$$I_P = W \times (31\ \text{mg/kJ}) \times \eta_{V_{th}} \times \eta_{H_2} \times \eta_{bio}, \quad [3]$$

where W is the total energy input in kilojoules, $\eta_{V_{th}} = 1.23\ \text{V}/E_{cell}$, η_{H_2} represents the faradaic efficiency for H_2 production, η_{bio} represents the efficiency of biomass production from H_2, and the

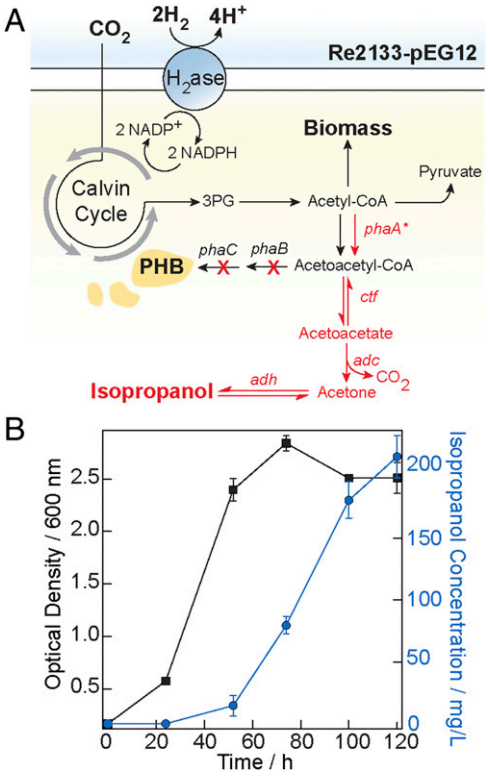

Fig. 5. Bioelectrochemical production of isopropanol. (*A*) Schematic diagram of *R. eutropha* strain *Re*2133-pEG12 containing an engineered pathway for isopropanol production (red lines, text) and grown on electrochemically produced H_2 and CO_2. The CoA transferase (*ctf*) reaction is reversible and coupled to production of succinyl-CoA from succinate. The alcohol dehydrogenase reaction (*adh*) is also reversible and coupled to proton transfer and NADPH oxidation (not shown for clarity). (*B*) Growth and isopropanol production in *Re*2133-pEG12 grown at 3.0 V with a 4-cm^2 CoP_i and 4-cm^2 SS304 anode and cathode, respectively. Error bars represent SEM; n = 3 independent experiments.

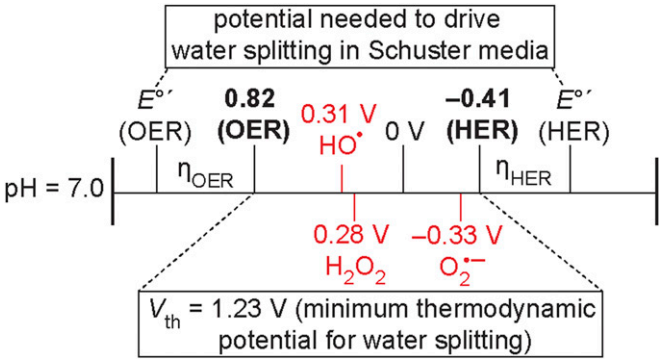

Fig. 6. Major ROS reactions at a cathode. The potentials (in V vs. NHE at pH 7.0) for water splitting are shown in the context of additional cell potentials associated with Eq. **1** and relative to the potentials of viable ROS. The additional potential associated with solution resistance is not shown for clarity.

maximum thermodynamic yields of biomass and isopropanol from input energy are 52 mgDCW/kJ and 31 mg/kJ, respectively (*SI Appendix*). The yield of biomass from electricity as a percentage of maximum thermodynamic yield was calculated as the total mass of biomass produced divided by ($W \times 52$ mgDCW/kJ) (Eq. **2**); isopropanol yield was calculated in a similar fashion using Eq. **3**. We calculated maximal yields of biomass and isopropanol for a single experiment to be 13.0 ± 0.9% (from the 2.7 V CoP_i | SS experiment in *SI Appendix*, Fig. S6) and 1.5 ± 0.2% (from Fig. 5), respectively. These were measured over the course of a complete experiment (4–5 d), including periods where growth was stalled due to a lag phase or to saturation. Maximal short-term yields of biomass and isopropanol, calculated over individual 24-h time periods, reached substantially greater levels (17.8 ± 1.2% and 3.9 ± 0.8%, respectively). As shown in *SI Appendix*, Fig. S7, these yields track the dependence of cell viability on E_{cell} potentials shown in Fig. 2. The biomass yields, shown in *SI Appendix*, Fig. S7, are significantly greater than those previously achieved in integrated bioelectrochemical systems (*SI Appendix*, Table S1), and the electricity-to-isopropanol yield is the highest solar-to-fuels yield (>300% as compared to previous studies) yet observed for an integrated bioelectrochemical system (*SI Appendix*, Table S1). These increased efficiencies are attributable in part to an increase in the $\eta_{V_{th}}$ term as a result of the ability of the CoP_i catalyst to perform at lower overpotential under bioelectrochemical conditions.

Assuming the electricity for cell growth were provided by an 18% efficient PV, the observed electricity-to-biomass efficiency would translate to a maximum equivalent solar-to-biomass efficiency of 2.3 ± 0.2% in the long term (4- to 5-d experiment), or 3.2 ± 0.2% in the short term (1 d maximum) and a short-term solar-to-fuel (isopropanol) yield of 0.7 ± 0.1%. These yields are on par with solar-to-biomass conversion efficiencies over a growing season for domestic C3 and C4 crops (2.9–4.3%); when photosynthetically active radiation is accounted for (48.7% of solar light energy available), the overall solar-to-biomass conversion efficiency is 1.4–2.1% (17, 18). Whereas the advantage of the bioelectrochemical and terrestrial crop yields are similar, bioelectrochemical systems such as the one reported here have the advantage that increased efficiencies may be realized with greater facility. Improvements in medium composition and reactor design (to lower Ω_{soln}), catalyst redesign for the HER reaction (to lower η_{HER}), continued biological engineering (to increase η_{bio}), and the steady improvement in solar PV design and efficiency will lead to continued increases in solar-to-fuels efficiency.

Conclusion

Liquid solar fuel derived from CO_2 holds promise as a both a storage mechanism for solar energy, and as a renewable, carbon-neutral, and infrastructure-compatible energy supply (2, 22, 28). Here, we demonstrate that an integrated bioelectrochemical system delivers appreciable electricity-to-biomass and electricity-to-fuel yields using scalable earth-abundant catalysts. Moreover, we have deciphered the need to maintain cell cultures at high cell potentials in previous studies. Whereas high potentials favor the use of cathodic current for HER, low potentials favor cathodic ROS production. At a sufficiently high potential, the ratio of HER to ROS production is high enough to favor biological growth over ROS toxicity. Owing to the relatively high overpotentials associated with the OER of noble metal electrodes in neutral-pH media, high cell potentials have been necessary to support biological growth for these catalysts. In the study reported herein, the potential at which cell growth is inhibited, owing in part to the lower η_{OER} associated with the CoP_i anode, is decreased. To this end, appreciable yields of biomass production from electricity (17.8% of thermodynamic maximum over 24 h in our highest-yielding experiment) were achieved. These results, in combination with engineered *R. eutropha*, have allowed us to create a fully integrated bioelectrochemical system for the production of isopropanol, a fusel alcohol compatible with current fuel infrastructure (46, 47), at up to 3.9% yield from electricity. Importantly, assuming a standard 18% PV were used to power our bioelectrochemical system, the maximal solar yields of biomass and isopropanol achieved (up to 3.2% and 0.7%, respectively) are commensurate with or greater than high-yielding domestic crops (17, 19). We note that the CoP_i OER catalyst may be coupled to a ternary metal alloy NiMoZn HER catalyst via a triple-junction amorphous silicon solar cell (40), to achieve direct solar-to-fuels conversion in a wireless "artificial leaf" format (30). In principle, adaptation of our bioelectrochemical system to such energy conversion constructs may provide a sustainable scheme for the conversion of sunlight, water, and CO_2 to liquid fuels.

Materials and Methods

Full details of all general methods, general reagents, and the preparation of materials and electrochemical cells used in this study are provided in *SI Appendix*.

Materials. *R. eutropha* H16 (wt) and *Re*2133-pEG12 were obtained from the Sinskey Laboratory at Massachusetts Institute of Technology. The latter is described by Grousseau et al. (42). Rich broth and minimal medium were prepared as previously described (21, 22). To grow *R. eutropha* strains electrochemically, glycerol stocks of the strain of interest were first streaked on rich broth plus Gm10 (plus Kan200 for *Re*2133-pEG12). Individual colonies were then grown in rich broth to saturation, diluted, and grown in fructose minimal medium to saturation, and then diluted and grown in carbon-free minimal medium under a hydrogen-containing atmosphere to an OD between 1 and 2. Cultures were then diluted to an OD between 0.17 and 0.22 in minimal medium before addition to the electrochemical cell. Full details of biological culture are provided in *SI Appendix*.

Catalyst depositions were conducted in 18-MΩ water using a CH Instruments model 760D potentiostat. The NiMoZn cathode fabricated by electrodepositing onto a substrate of either plainer SS, 304 SS mesh, or nickel mesh using a previously reported procedure (40). The CoP_i catalyst was deposited by bulk electrolysis (35) in a two-compartment electrochemical cell with a glass frit junction of fine porosity. Electrolysis was carried out at 0.85 V vs. Ag/AgCl until the desired amount of charge was passed. Typically, 100 mC of charge was passed for a 2-cm^2 electrode. Deposition times were typically ~1 h.

Bioelectrochemical Reactors. For H-cell experiments, minimal medium cultures of *R. eutropha* were added to each of two (anode/cathode) chambers in an H cell separated by a 0.45-μm surfactant-free cellulose acetate (SFCA) filter to prevent exchange of microbes between them. Each chamber was magnetically stirred at 200 rpm and maintained at room temperature. In single-cell

experiments, minimal medium cultures of *R. eutropha* were added to a sterile 40-mL glass vial fitted with a rubber septum and a glass sparger connected to a CO_2 tank by a 0.45-μm SFCA filter. Phosphate buffer (minimal medium) and sparged CO_2 were sufficient to maintain culture pH in the range of 6.5–7.5. Sterile electrodes were inserted through the rubber septum, a magnetic stir bar (Squid model stir plate from IKA; Staufen, Germany) was used to mix the culture at 250 rpm, and a water bath was used to keep the setup at 30 °C. Up to eight electrochemical cells were controlled simultaneously and potentiostatically using a Gamry Reference 600 potentiostat and ECM 8 multiplexer. Full details are provided in *SI Appendix, SI Materials and Methods*.

Assays and Analysis. Spot assays were performed on 100 μL of culture, diluted 1:10 in fresh minimal medium, and vortexed. Four serial 10-fold dilutions were made of this sample, and 2 μL of each dilution spotted on rich broth agar plates and allowed to dry on the bench top. Plates were typically grown for 2 d at 30 °C before imaging.

H_2O_2 was measured in a 96-well plate format using the Amplex Red H_2O_2 Detection Kit (Sigma-Aldrich), which specifically detects H_2O_2 via an enzymatic assay (*SI Appendix, SI Materials and Methods*), according to the manufacturers' instructions. H_2O_2 was quantified by comparing absorbance at 555 nm to a standard curve generated from H_2O_2 standards ranging from 0 to 40 μM. See *SI Appendix, SI Materials and Methods* for full details.

HPLC of culture supernatants was performed on an Agilent HPLC 1200 equipped with an Aminex HPX-87H column and using a 0.00125 M H_2SO_4 mobile phase. UV and refractive index detection were used to identify and quantify pyruvate, acetone, and isopropanol. See *SI Appendix, SI Materials and Methods* for full details.

Electrode performance was compared using Tafel analysis conducted using multicurrent step measurements between 5 mA and 1 μA allowing between 300 and 1,200 s for equilibration between steps. Solution resistance was measured, and resistive voltage contributions were subtracted from the total measured OER overpotential. All Tafel measurements were conducted in a two-compartment electrochemical cell with a glass frit junction of fine porosity. The Tafel slope for CoP_i on SS304 was 75 mV/dec, in good agreement with previously reported values. Additional Tafel analysis was conducted to compare CoP_i performance in growth media and 0.5 M phosphate buffer. Tafel slopes for KP_i and minimal growth medium were 71 and 79 mV/dec, indicating no significant change in OER performance between solutions.

ACKNOWLEDGMENTS. We thank J. Lu and A. J. Sinskey for plasmids and reagents; J. Lu, T. J. Kempa, D. C. MacKellar, C. R. Cox, and T. J. Ford for helpful discussion; and A. Todd for providing custom software to operate the Gamry potentiostat and multiplexer. This work was supported by Air Force Office of Scientific Research Grant FA9550-09-1-0689 (to D.G.N.), Office of Naval Research Multidisciplinary University Research Initiative Award N00014-11-1-0725 (to P.A.S.), and a National Science Foundation Graduate Research Fellowship (to J.P.T.). We thank TomKat Trust for funding of the First 100 Watts Project.

1. Lewis NS, Nocera DG (2006) Powering the planet: Chemical challenges in solar energy utilization. *Proc Natl Acad Sci USA* 103(43):15729–15735.
2. Cook TR, et al. (2010) Solar energy supply and storage for the legacy and nonlegacy worlds. *Chem Rev* 110(11):6474–6502.
3. Turkenburg W (2012) *Global Energy Assessment—Toward a Sustainable Future* (Cambridge Univ Press, Cambridge, UK), pp 761–900.
4. Tanaka M (2006) Real-time pricing with ramping costs: A new approach to managing a steep change in electricity demand. *Energy Policy* 34(18):3634–3643.
5. Sovacool BK (2009) The intermittency of wind, solar, and renewable electricity generators: Technical barrier or rhetorical excuse? *Util Policy* 17(3):288–296.
6. International Energy Agency (2006) *Hydrogen Production and Storage—R&D Priorities and Gaps* (International Energy Agency, Paris).
7. Genovese JE, Harg K, Paster M, Turner JA (2009) *Current (2009) State-of-the-Art Hydrogen Production Cost Estimate Using Water Electrolysis: Independent Review* (National Renewable Energy Laboratory, Golden, CO).
8. Hori Y, Murata A, Takahashi R (1989) Formation of hydrocarbons in the electrochemical reduction of carbon dioxide at a copper electrode in aqueous solution. *J Chem Soc Faraday Trans I* 85(8):2309–2326.
9. Kuhl KP, Cave ER, Abram DN, Jaramillo TF (2012) New insights into the electrochemical reduction of carbon dioxide on metallic copper surfaces. *Energy Environ Sci* 5:7050–7059.
10. Chen Y, Li CW, Kanan MW (2012) Aqueous CO_2 reduction at very low overpotential on oxide-derived Au nanoparticles. *J Am Chem Soc* 134(49):19969–19972.
11. Li CW, Ciston J, Kanan MW (2014) Electroreduction of carbon monoxide to liquid fuel on oxide-derived nanocrystalline copper. *Nature* 508(7497):504–507.
12. Li CW, Kanan MW (2012) CO_2 reduction at low overpotential on Cu electrodes resulting from the reduction of thick Cu_2O films. *J Am Chem Soc* 134(17):7231–7234.
13. Medina-Ramos J, DiMeglio JL, Rosenthal J (2014) Efficient reduction of CO_2 to CO with high current density using in situ or ex situ prepared Bi-based materials. *J Am Chem Soc* 136(23):8361–8367.
14. Savage DF, Way J, Silver PA (2008) Defossiling fuel: How synthetic biology can transform biofuel production. *ACS Chem Biol* 3(1):13–16.
15. Machado IMP, Atsumi S (2012) Cyanobacterial biofuel production. *J Biotechnol* 162(1):50–56.
16. Wang B, Wang J, Zhang W, Meldrum DR (2012) Application of synthetic biology in cyanobacteria and algae. *Front Microbiol* 3(344):344.
17. Blankenship RE, et al. (2011) Comparing photosynthetic and photovoltaic efficiencies and recognizing the potential for improvement. *Science* 332(6031):805–809.
18. Walker DA (2009) Biofuels, facts, fantasy, and feasibility. *J Appl Phycol* 21(5):509–517.
19. Zhu XG, Long SP, Ort DR (2010) Improving photosynthetic efficiency for greater yield. *Annu Rev Plant Biol* 61:235–261.
20. Schlegel HG, Lafferty R (1965) Growth of "knallgas" bacteria (*Hydrogenomonas*) using direct electrolysis of the culture medium. *Nature* 205:308–309.
21. Schuster E, Schlegel HG (1967) Chemolithotrophes wachstum von hydrogenomonas H16 im chemostaten mit elektrolytischer knallgaserzeugung. *Arch Microbiol* 58(4):380–409.
22. Kanan MW, Nocera DG (2008) In situ formation of an oxygen-evolving catalyst in neutral water containing phosphate and Co^{2+}. *Science* 321(5892):1072–1075.
23. Kanan MW, et al. (2010) Structure and valency of a cobalt-phosphate water oxidation catalyst determined by in situ X-ray spectroscopy. *J Am Chem Soc* 132(39):13692–13701.
24. Du P, Kokhan O, Chapman KW, Chupas PJ, Tiede DM (2012) Elucidating the domain structure of the cobalt oxide water splitting catalyst by X-ray pair distribution function analysis. *J Am Chem Soc* 134(27):11096–11099.
25. Farrow CL, Bediako DK, Surendranath Y, Nocera DG, Billinge SJL (2013) Intermediate-range structure of self-assembled cobalt-based oxygen-evolving catalyst. *J Am Chem Soc* 135(17):6403–6406.
26. Surendranath Y, Dincă M, Nocera DG (2009) Electrolyte-dependent electrosynthesis and activity of cobalt-based water oxidation catalysts. *J Am Chem Soc* 131(7):2615–2620.
27. Surendranath Y, Lutterman DA, Liu Y, Nocera DG (2012) Nucleation, growth, and repair of a cobalt-based oxygen evolving catalyst. *J Am Chem Soc* 134(14):6326–6336.
28. Lutterman DA, Surendranath Y, Nocera DG (2009) A self-healing oxygen-evolving catalyst. *J Am Chem Soc* 131(11):3838–3839.
29. Kanan MW, Surendranath Y, Nocera DG (2009) Cobalt-phosphate oxygen-evolving compound. *Chem Soc Rev* 38(1):109–114.
30. Esswein AS, Surendranath Y, Reece SY, Nocera DG (2011) Highly active cobalt phosphate and borate based oxygen evolving anodes operating in neutral and natural waters. *Energy Environ Sci* 4:499–504.
31. Li H, et al. (2012) Integrated electromicrobial conversion of CO_2 to higher alcohols. *Science* 335(6076):1596.
32. Nevin KP, et al. (2011) Electrosynthesis of organic compounds from carbon dioxide is catalyzed by a diversity of acetogenic microorganisms. *Appl Environ Microbiol* 77(9):2882–2886.
33. Lovley DR (2011) Powering microbes with electricity: Direct electron transfer from electrodes to microbes. *Environ Microbiol Rep* 3(1):27–35.
34. Khunjar WO, Sahin A, West AC, Chandran K, Banta S (2012) Biomass production from electricity using ammonia as an electron carrier in a reverse microbial fuel cell. *PLoS One* 7(9):e44846.
35. Yunker SB, Radovich JM (1986) Enhancement of growth and ferrous iron oxidation rates of *T. ferrooxidans* by electrochemical reduction of ferric iron. *Biotechnol Bioeng* 28(12):1867–1875.
36. Rabaey K, Rozendal RA (2010) Microbial electrosynthesis—revisiting the electrical route for microbial production. *Nat Rev Microbiol* 8(10):706–716.
37. Nevin KP, Woodard TL, Franks AE, Summers ZM, Lovley DR (2010) Microbial electrosynthesis: Feeding microbes electricity to convert carbon dioxide and water to multicarbon extracellular organic compounds. *MBio* 1(2):e00103.
38. Bauer D, et al. (2011) *Critical Materials Strategy* (US Department of Energy, Washington, DC).
39. Nocera DG (2012) The artificial leaf. *Acc Chem Res* 45(5):767–776.
40. Reece SY, et al. (2011) Wireless solar water splitting using silicon-based semiconductors and earth-abundant catalysts. *Science* 334(6056):645–648.
41. Zhang Y, Merrill MD, Logan BE (2010) The use and optimization of stainless steel mesh cathodes in microbial electrolysis cells. *Int J Hydrogen Energy* 35(21):12020–12028.
42. Grousseau E, Lu J, Gorret N, Guillouet SE, Sinskey AJ (2014) Isopropanol production with engineered *Cupriavidus necator* as bioproduction platform. *Appl Microbiol Biotechnol* 98(9):4277–4290.
43. Mansfield DA, Anderson AJ, Naylor LA (1995) Regulation of PHB metabolism in *Alcaligenes eutrophus*. *Can J Microbiol* 41(13):44–49.
44. Steinbuchel A, Schlegel HG (1989) Excretion of pyruvate by mutants of *Alcaligenes eutrophus*, which are impaired in the accumulation of poly(beta-hydroxybutyric acid) (PHB), under conditions permitting synthesis of PHB. *Appl Microbiol Biotechnol* 31(2):168–175.
45. Sawyer DT (1991) *Oxygen Chemistry* (Oxford Univ Press, New York), p 21.
46. Peralta-Yahya PP, Keasling JD (2010) Advanced biofuel production in microbes. *Biotechnol J* 5(2):147–162.
47. Connor MR, Liao JC (2009) Microbial production of advanced transportation fuels in non-natural hosts. *Curr Opin Biotechnol* 20(3):307–315.